Earth's Future

RESEARCH ARTICLE

Key Points:

- Hotspots for high land surface temperatures (LSTs) were globally identified using a physically based analytical approach incorporating land and atmospheric conditions
- High LSTs primarily occur in Middle East and North Africa with values exceeding 85°C
- Maximum LSTs rising at a rate of 0.17°C/decade may limit plant growth and biological adaptability in a warming world

Supporting Information:

Supporting Information may be found in the online version of this article.

Correspondence to:

M. Aminzadeh and N. Shokri,
milad.aminzadeh@tuhh.de;
nima.shokri@tuhh.de

Author Contributions:

Conceptualization: Milad Aminzadeh, Dani Or, Bjorn Stevens, Amir AghaKouchak, Nima Shokri
Formal analysis: Milad Aminzadeh
Investigation: Milad Aminzadeh, Dani Or, Bjorn Stevens, Amir AghaKouchak, Nima Shokri
Methodology: Milad Aminzadeh, Dani Or, Bjorn Stevens, Amir AghaKouchak, Nima Shokri

Upper Bounds of Maximum Land Surface Temperatures in a Warming Climate and Limits to Plant Growth

Milad Aminzadeh[1] [iD], **Dani Or[2,3]** [iD], **Bjorn Stevens[4]** [iD], **Amir AghaKouchak[5]** [iD], and **Nima Shokri[1]** [iD]

[1]Institute of Geo-Hydroinformatics, Hamburg University of Technology, Hamburg, Germany, [2]Division of Hydrologic Sciences, Desert Research Institute, Reno, NV, USA, [3]Department of Environmental Systems Science, ETH Zurich, Zurich, Switzerland, [4]Max Planck Institute for Meteorology, Hamburg, Germany, [5]Department of Civil and Environmental Engineering, University of California, Irvine, CA, USA

Abstract Extremely high land surface temperatures affect soil ecological processes, alter land-atmosphere interactions, and may limit some forms of life. Extreme surface temperature hotspots are presently identified using satellite observations or deduced from complex Earth system models. We introduce a simple, yet physically based analytical approach that incorporates salient land characteristics and atmospheric conditions to globally identify locations of extreme surface temperatures and their upper bounds. We then provide a predictive tool for delineating the spatial extent of land hotspots at the limits to biological adaptability. The model is in good agreement with satellite observations showing that temperature hotspots are associated with high radiation and low wind speed and occur primarily in Middle East and North Africa, with maximum temperatures exceeding 85°C during the study period from 2005 to 2020. We observed an increasing trend in maximum surface temperatures at a rate of 0.17°C/decade. The model allows quantifying how upper bounds of extreme temperatures can increase in a warming climate in the future for which we do not have satellite observations and offers new insights on potential impacts of future warming on limits to plant growth and biological adaptability.

Plain Language Summary While satellite imagery can identify extreme land surface temperatures, land and atmospheric conditions for the onset of maximum land surface temperature (LST) have not yet been globally explored. We developed a physically based analytical model for quantifying the value and spatial extent of maximum LST and provide insights into combinations of land and atmospheric conditions for the onset of such temperature extremes. Results show that extreme LST hotspots occur primarily in the Middle East and North Africa with highest values near 85°C. Importantly, persistence of surface temperatures exceeding 75°C limits vegetation growth and disrupts primary productivity such as in Lut desert in Iran. The study shows that with global warming, regions with prohibitive land surface temperatures will expand.

1. Introduction

Record-breaking extreme heats of summer 2022 underlined the issues facing societies tasked with adapting to a warmer climate observed all around the world. Deadly heatwaves of south Asia, hottest May on record in France, the first-ever national emergency red heat alert declared by the UK and devastating summer wildfire in California are only a few examples illustrating the world is actually warming. This reality has ceased to be a scientific abstraction discussed by panels of scientists, it is now felt by the public (Masson-Delmotte et al., 2021). The changes in frequency, intensity, spatial extent and duration of extreme events such as the recent European severe summer heatwaves and drought (Büntgen et al., 2021) will lead to change in all drivers shaping biosphere and the life on the Earth. This highlights the importance of developing predictive tools to identify intensity, frequency, and distribution of climate extremes.

Heat extremes and the increase in land surface temperature (LST) are only a few implications of the anthropogenic climate change influencing climatological, hydrological, and ecological processes across scales, which is the focus of the present study. Surface temperature is at the core of longwave radiation and turbulent exchanges of heat and water vapor between land surface and atmosphere, and thus influences regional and global climate patterns (Aminzadeh & Or, 2014; Chen et al., 2011). High values of LST affect surface fluxes and land-atmosphere interactions and may reinforce extreme events such as heatwaves and wildfires (Aminzadeh et al., 2021; Miralles et al., 2014; Pietikäinen et al., 2005). It can further impose limitations on ecological processes. Evidence suggests

the upper limits of LST for desert vegetation is about 70°C, as at warmer temperatures plant tissues are not evolved to withstand the heat (Nobel et al., 1986).

Currently, identification of maximum LST hotspots relies largely on remote sensing and satellite observations, or reanalyses estimates derived from complex climate models with Earth system components (Azarderakhsh et al., 2020; Li et al., 2013; Mildrexler et al., 2011; Zhao et al., 2021). Temperature hotspots might be underestimated and overlooked by spatial/temporal aggregation in satellite imagery or in modeling approaches that are inherently designed to quantify a wide range of coupled land, ocean, and atmospheric variables over large scales, and using parametrizations designed to damp extremes. These limit predictability of the location and the extent of maximum surface temperatures that could affect human, plants, and wildlife adaptability thresholds, especially in the context of a changing climate.

In this study, we seek to quantify land and atmospheric conditions for the onset of maximum LST and relate it to the limit of life in places where record temperatures have been observed (e.g., Lut Desert in Iran, known as the thermal pole of the Earth parts of which are devoid of plants (Stone, 2016)). Two aspects are important in this study: (a) where do surface temperature hotspots occur and what are the maximum values of LSTs? (b) what are the ecological ramifications of such high LSTs especially with respect to limiting plant life as for example, observed in Lut Desert (Stone, 2016). We develop a physically based analytic model incorporating effects of land characteristics and atmospheric forcing conditions to identify hotspots for maximum temperatures on a global scale. Inherent land characteristics (e.g., land cover, elevation, soil type) along with atmospheric forcing variables are used to quantify maximum surface temperatures in summer months from 2005 to 2020 at a global scale. This allows us to predict the extent of temperature extremes in 2,100 under two contrasting greenhouse gas emission scenarios of Shared Socioeconomic Pathways, that is, SSP1-2.6 (high mitigation) and SSP5-8.5 (high emission) in the Coupled Model Intercomparison Project Phase 6 (CMIP6).

2. Methods and Data

2.1. A Closed-Form Equation for Dry Soil Surface Temperature

Bare soil surfaces with low values of thermal conductivity and albedo, subjected to high values of radiation and low prevailing wind speeds are likely to attain highest temperatures (Azarderakhsh et al., 2020; Garratt, 1992; Kubecka, 2001; Mildrexler et al., 2011). The implicit assumption is that barren surfaces in hot regions remain mostly at stage-2 evaporation (except following episodic rainfall events) with vapourization taking place below the surface (Lehmann et al., 2019; Shokri & Or, 2011). This supports a negligible evaporation cooling at the surface and formation of high temperatures over dry surfaces (Aminzadeh & Or, 2013; Lehmann et al., 2008, 2019). This enables us to apply an energy constrained closed-form equation to quantify upper limits of maximum LSTs over bare soil surfaces under different climatic conditions. Surface energy balance over dry soil surfaces with negligible latent heat cooling (LE = 0) is thus written as:

$$R_n = H + G \tag{1a}$$

$$(1 - \alpha)R_{s,\text{in}} + \sigma \varepsilon_s \varepsilon_a T_a^4 - \sigma \varepsilon_s T_s^4 = \frac{k_a}{\delta}(T_s - T_a) + \frac{k_{\text{soil}}}{Z}(T_s - T_{\text{soil}}) \tag{1b}$$

where R_n, H, and G, are net radiation, sensible heat, and soil heat flux, respectively; $R_{s,\text{in}}$ is the incoming shortwave radiation flux; α is surface albedo; σ is the Stefan-Boltzmann constant; ε_s and ε_a are surface and atmospheric emissivity, respectively (Brutsaert, 1982; Herrero & Polo, 2012); δ is the thickness of air viscous sublayer (i.e., a function of wind speed) (Haghighi & Or, 2013); T_s is surface temperature; T_a is air temperature; and k_a is the air thermal conductivity. A comprehensive representation of subsurface thermal regimes requires solution of energy balance equation in soil profile with certain assumptions about soil thermal characteristics and moisture content in depth. Following Shahraeeni and Or (2011), we opted for a linearized soil temperature profile to retain applicability of the model at global scale. For (sinusoidal) diurnal variations of soil temperature, the thermal decay depth below the surface is estimated as (Jury & Horton, 2004):

$$Z = \sqrt{\frac{P D_T}{\pi}} \tag{2}$$

where P is the period of sinusoidal surface temperature variations (24 hr) and D_T is the effective thermal diffusivity of dry soil (m²/h). The corresponding soil temperature at thermal decay depth (T_{soil}) is estimated as the mean daily air temperature. Thermal conductivity of dry soil (k_{soil}) can be estimated as a function of clay fraction (ϕ_c) and soil bulk density (ρ_b) (He et al., 2021):

$$k_{soil} = 0.141 \times 1.005^{\phi_c} \rho_b^{1.481} \tag{3}$$

Linearization of surface longwave radiation flux around air temperature allows us to provide a closed-form equation for quantification of maximum LSTs (Shahraeeni & Or, 2011):

$$\sigma \varepsilon_s T_s^4 = 4\sigma \varepsilon_s T_a^3 T_s - 3\sigma \varepsilon_s T_a^4 \tag{4}$$

$$T_s = \frac{(1-\alpha)R_{s,in} + (3+\varepsilon_a)\sigma \varepsilon_s T_a^4 + \frac{k_a}{\delta}T_a + \frac{k_{soil}}{z}T_{soil}}{4\sigma \varepsilon_s T_a^3 + \frac{k_a}{\delta} + \frac{k_{soil}}{z}} \tag{5}$$

Equation 5 incorporates the impacts of land characteristics and atmospheric forcing parameters for estimating maximum land surface temperatures.

Note that accurate estimation of surface temperature requires investigation of complex land-atmosphere thermal feedback processes (considering variability of turbulent scaling parameters for proper estimates of aerodynamic resistances) coupled with subsurface thermal regimes through numerical schemes similar to one proposed by Garratt (1992). While complexity of numerical solutions (with several parametrizations) may hinder quantification of maximum LSTs at global scale, the simple, yet physically based Equation 5 provides an analytical basis to globally estimate upper bounds of LST without getting bogged down in details of land-atmosphere interactions (Aminzadeh et al., 2016; Hobbins et al., 2001) and surface transfer characteristics considering the global extent of barren surfaces.

2.2. Land Characteristics and Meteorological Data

To focus the study on barren soil surfaces, yearly land cover data sets were obtained from the Terra and Aqua combined Moderate Resolution Imaging Spectroradiometer (MODIS) Land Cover Climate Modeling Grid (MCD12C1) Version 6 at spatial resolution of 0.05° × 0.05° (Friedl & Sulla-Menashe, 2015). Surface albedo and emissivity, and hourly meteorological data including air temperature, wind speed, shortwave irradiation, near surface specific humidity, and air pressure were obtained from the Modern-Era Retrospective analysis for Research and Applications, Version 2 (MERRA-2) at spatial resolution of 0.625° × 0.5° for the period of 2005–2020 (Gelaro et al., 2017; Global Modeling and Assimilation Office (GMAO), 2015a, 2015b).

We extracted surface soil type information and bulk density from the Harmonized World Soil Database (HWSD) v1.2 at spatial resolution of 0.05° × 0.05° (Wieder et al., 2014). Land elevation data were obtained from Global Multi-resolution Terrain Elevation Data (Danielson & Gesch, 2011) at resolution of 0.25° × 0.25°. Downscaled future climate data under SSP1-2.6 and SSP5-8.5 at 0.25° × 0.25° spatial resolution were downloaded from NASA Earth Exchange Global Daily Downscaled Projections (NEX-GDDP-CMIP6) (Thrasher et al., 2022). While SSP1-2.6 represents a future pathway under low emission of greenhouse gases (GHGs) with 2.6 W/m² increase in radiative forcing by the end of the 21st century, SSP5-8.5 remarks a contrasting global warming condition with a substantial emission of GHGs causing 8.5 W/m² increase in radiative flux (Riahi et al., 2017). Considering different spatial resolution of land and atmospheric data, surface radiative properties and meteorological data from MERRA-2, land elevation data of GMTED, and future meteorological forcing data were interpolated to 0.05° × 0.05° rectangular grid using bilinear method.

3. Results

3.1. A Physically Based Framework for Predicting Maximum LST

To evaluate our physically based framework for estimating upper bounds and identifying local maximum surface temperatures based on salient land characteristics and atmospheric conditions, global temperature hotspots of the Earth identified based on MODIS Aqua LST (MYD11A1 V6) at 1 km spatial resolution were used.
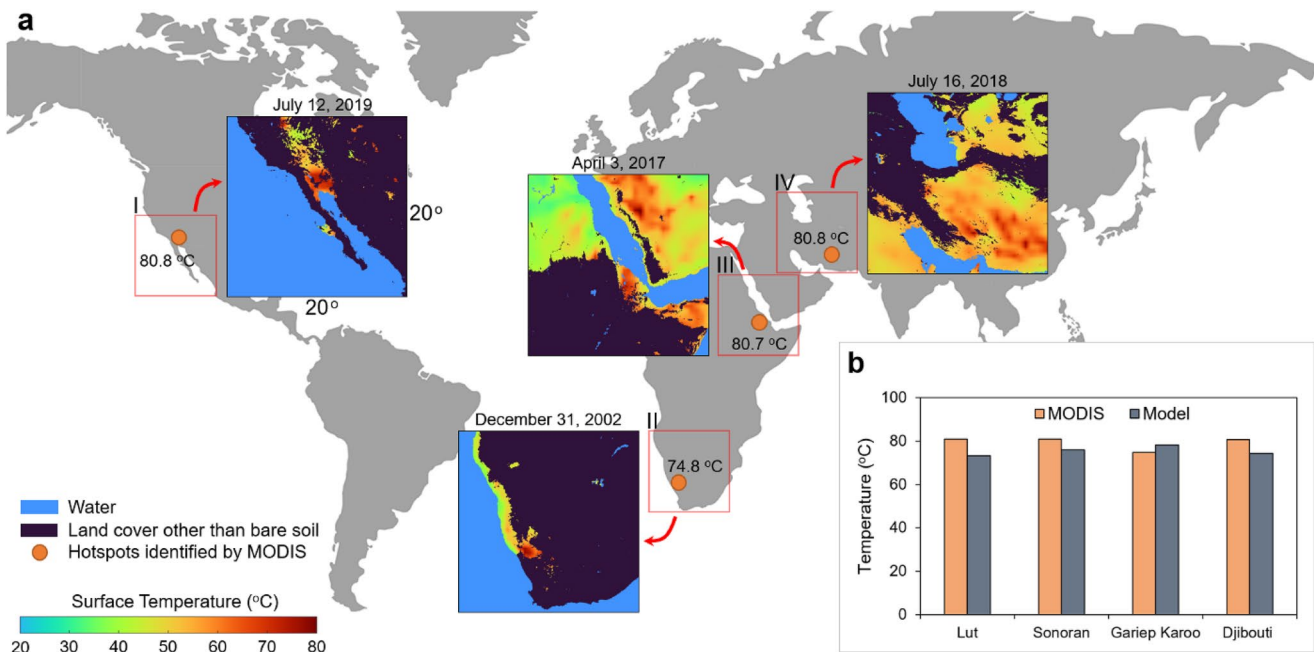
Figure 1. Analytically estimated local maximum land surface temperatures versus satellite observations. (a) Model estimates of the spatial variation of maximum temperature over bare soil surfaces in a 20° × 20° window encompassing hotspots in Sonoran Desert (I), Gariep Karoo Desert (II), Djibouti (III), and Lut Desert (IV) identified from MODIS Aqua land surface temperature data (2002–2019) (Zhao et al., 2021). (b) Comparison between model estimates and MODIS observations of the temperature of hotspots in Sonoran Desert, Gariep Karoo Desert, Djibouti, and Lut Desert. Atmospheric forcing variables for model calculations were extracted from MERRA-2 reanalysis data.

According to Zhao et al. (2021) analyzing MODIS data from 2002 to 2019, extremely high LSTs have been identified in Lut Desert (80.8°C on 16 July 2018), Sonoran Desert (80.8°C on 12 July 2019), Gariep Karoo Desert (74.8°C on 31 December 2002), and Djibouti (80.7°C on 3 April 2017) at 13:30 local time associated with satellite overpass (Figure 1). Land characteristics and hourly meteorological data from the Modern-Era Retrospective analysis for Research and Applications, Version 2 (MERRA-2) were used to estimate location of hotspots in a 20° × 20° window encompassing these places and quantify corresponding local maximum surface temperatures. Figure 1 depicts model predictions of the location of hotspots (focusing on bare soil surfaces with 0.05°×0.05° spatial resolution) and their maximum temperatures in Lut Desert, Sonoran Desert, Gariep Karoo Desert, and Djibouti in the above-mentioned dates at 13:30 local time compared with the measurement reported by Zhao et al. (2021) based on MODIS data.

Historical MODIS measurements of maximum LSTs in these four hottest places on Earth from 2002 to 2019 (Zhao et al., 2021) were further compared with model estimates of the variation of maximum surface temperature with radiative flux (Figure S1a in Supporting Information S1). According to atmospheric forcing variables of these hotspots (extracted from MERRA-2 reanalysis data), extremely high LSTs are bounded to high radiative forcing (incoming shortwave radiation of 800–1,100 W/m²) and low advective flows (lateral wind speeds of 0.5–4 m/s). The explicit analytical formulation of maximum surface temperature thus enables clear attribution of the relations between maximum LST and primary atmospheric variables (Supporting Information S1). The findings in Figure S1 in Supporting Information S1 highlight the important effect of low wind speeds (strong nonlinear relations across narrow range of low wind speeds <5 m/s for high radiation regimes) reflecting the central role of turbulent heat exchanges between land and atmosphere in shaping maximum LSTs. In contrast to the positive response of surface temperature to increasing air temperature and radiation flux, variations in wind speed can increase or decrease surface temperature depending on the prevailing radiation regime.

3.2. Quantifying Global Hotspots of Maximum LST

Analysis of MODIS observations of maximum LSTs (Figure 1) indicate that these hotspots are associated with barren surfaces (absence of vegetation), at low elevations (<1,000 m) where local topography limits air

flows and contributes to low turbulent exchanges. These cues helped us with delineating potential regions for high LST sharing similar characteristics (i.e., land cover type and elevation in land surfaces from 130° W to 160° E and 40° S to 60° N), and using available meteorological data to identify places that may attain high values of LSTs. Air temperature, wind speed, and shortwave radiation are primary atmospheric forcing parameters that govern maximum temperature of bare soil surfaces (Garratt, 1992; Nobel et al., 1986). Considering the coupling between LST and near surface air temperature (through sensible heat feedback mechanisms) (Aminzadeh et al., 2016; Aminzadeh & Or, 2017; Mildrexler et al., 2011), we primarily focused on the influence of wind and radiation in shaping extremely high LSTs. Wind speed (at 2 m height) and incoming shortwave radiation data during summers (June, July, August in northern hemisphere and December, January, February in southern hemisphere) between 13:00 to 14:00 local time (when maximum LSTs often occur (Sharifnezhadazizi et al., 2019)) from 2005 to 2020 were extracted from global MERRA-2 data sets. The mean values of wind and radiation over land surfaces (excluding oceans) for the mentioned period were thus determined as 5.1 m/s and 752 W/m^2, respectively.

We have identified potential locations for attainment of maximum LST as bare soil surfaces with elevations less than 1,000 m (limiting the primary impact of air temperature lapse rate that could explicitly affect LST) subjected to wind speeds lower than the mean value of 5.1 m/s and shortwave radiation greater than the mean value of 752 W/m^2. These regions are delineated in Figure 2. Our analysis shows that these regions that cover more than 7.5 million km^2 of the land surface are most susceptible to very high surface temperatures (consistent with satellite-based hotspots reported in Zhao et al. (2021) and Mildrexler et al. (2011)). While temperature hotspots are distributed globally, they aggregate in latitudes between 13° to 43° N (mainly covering Middle East and North Africa). These regions are characterized by persistence of clear skies, calm winds, and low precipitations arising from high pressure atmospheric systems in subtropical ridge (mid-latitudes around ±30°) (Wang et al., 2022; Zhao et al., 2021). Such conditions favor occurrence of extreme high surface temperatures as we show theoretically.

Our theoretical framework validated in Figure 1 was employed to predict LST hotspots and their magnitudes on a global scale. Maximum temperature of hotspots obtained from daily analysis for 13:00 to 14:00 local time, during summers from 2005 to 2020 are depicted in Figure 3. Regions with extremely high LSTs exceeding 80°C are observed in Pakistan, Iran, western and eastern Arabian Peninsula, Niger, south of Namibia, and west of the United States (California). Figure 3b summarizes the number of days that surface temperature exceeded 90% of the maximum LST of each map cell (pixel) during ∼1,440 summer days (2005–2020). According to Figure 3b, hotspots in Afghanistan, Pakistan, Iran, and eastern Arabian Peninsula have experienced surface temperatures exceeding 90% of local maximum LSTs for more than 100 days. The theoretical calculations of maximum LST were obtained assuming a negligible evaporative flux (i.e., dry bare soil) thus providing an upper limit for local surface temperatures; however, soil moisture and thus latent heat losses are important ingredients in limiting occurrence of high LSTs.

Yearly analyses of maximum LSTs from 2005 to 2020, shows that the global average of maximum LST of hotspots is increasing at a rate of 0.17°C/decade (Figure 3c). For the same period (2005–2020), NOAA GlobalTemp data set indicates 0.34°C/decade increase in global mean LST (note the long term investigation of LST anomalies from 1950 to 2020 shows 0.22°C/decade increase in global mean LST) (NCEI, 2022). Given that maximum LST hotspots are located primarily in barren regions less affected by direct anthropogenic activities, it is interesting to see that factors affecting global mean LST (GHG emissions, urbanization, and land use/land cover changes) propagate to extreme values of LST (Tran et al., 2017). In the following, we address the extent of maximum LST expansion with projected climate change.

3.3. Maximum Surface Temperatures in a Changing Climate

While atmospheric behavior in a changing climate is widely addressed in different global climate models, land response to global warming remains a grand challenge (Lacis et al., 2010; Webb et al., 2017). We thus harness the proposed physically based framework to predict the extent of maximum land surface temperatures in a changing climate. We made use of the downscaled atmospheric forcing data derived from different climate scenarios in the Max Planck Institute Earth System Model (MPI-ESM, version 1.2 in its high-resolution) under CMIP6 (Mauritsen et al., 2019; Thrasher et al., 2022).
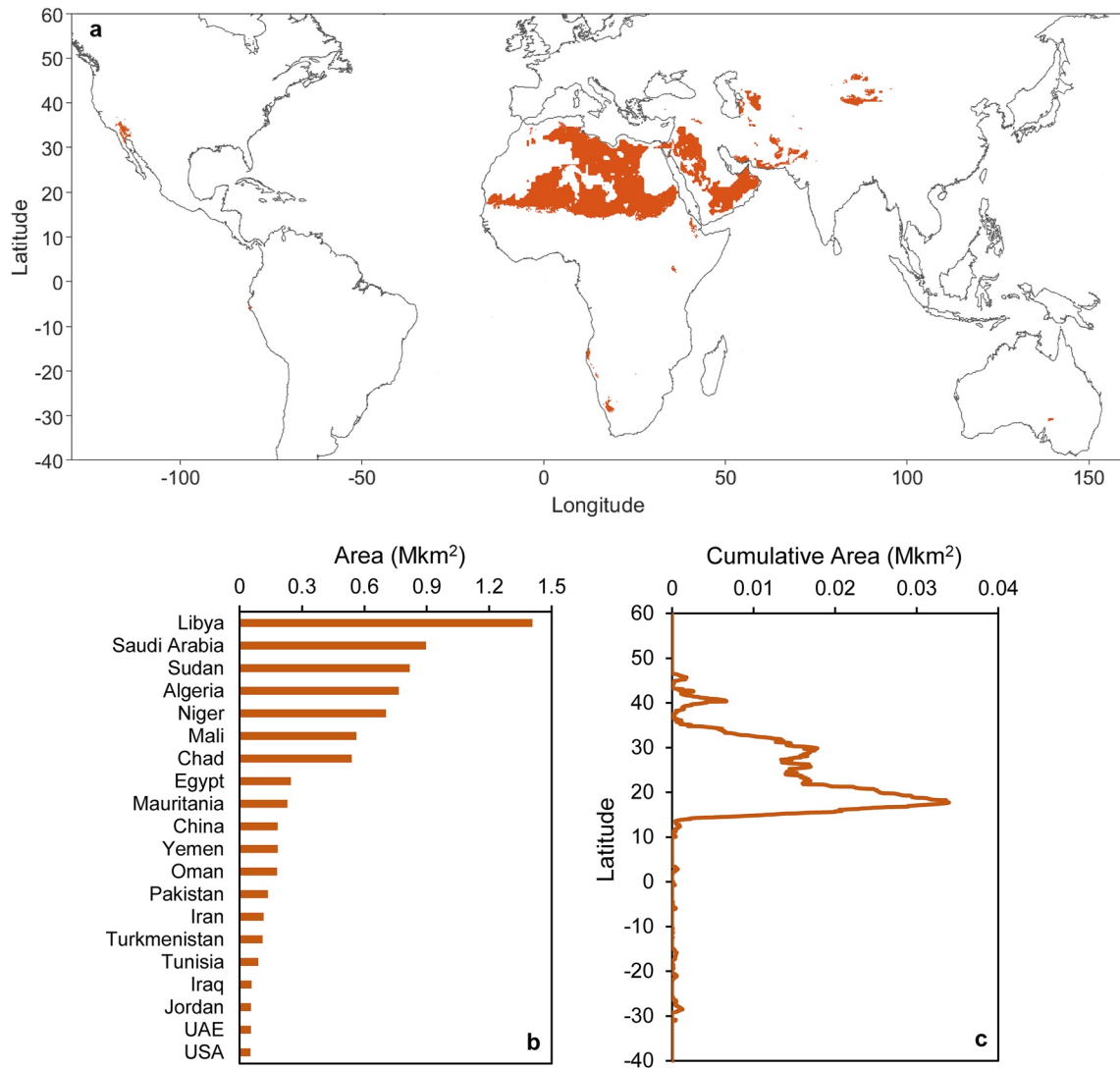
Figure 2. (a) Model estimates of the locations of land surface temperature hotspots deduced from land characteristics (bare soil surfaces with elevation <1,000 m) and meteorological forcing parameters (wind <5.1 m/s and incoming shortwave radiation >752 W/m²); (b) the top 20 countries with highest area of temperature hotspots; (c) cumulative area of hotspots by latitude indicating that temperature hotspots covering more than 7.5 Mkm² of the land surface are mostly located between 13° to 43° N.

Considering the lack of hourly atmospheric forcing variables in CMIP6 future climate scenarios, we used daily values of wind and radiation and the maximum air temperature (of each day) to investigate changes in the maximum LST of hotspots in 2100 relative to 2020 under SSP1-2.6 and SSP5-8.5 (Figure 4). Note that daily values of atmospheric forcing (especially radiation) obtained from downscaled future climate data may not represent the real condition (mid-day extremes) for occurrence of high surface temperatures; nevertheless, the idea here is to delineate relative changes in maximum LSTs from 2020 to 2100 under the same forcing condition obtained from MPI-ESM (for 2020 and 2100). While some hotspots in central Sahara Desert (Libya, Chad, Niger), northwestern China (Taklamakan Desert), and eastern Arabian Peninsula (Oman and United Arab Emirates) will experience lower maximum temperatures in 2100 relative to 2020 under SSP1-2.6, the results based on SSP5-8.5 indicate a considerable increase in maximum LSTs in 2100. In particular, some barren surfaces in Tunisia, Algeria, Saudi Arabia, Iran, Afghanistan, and Pakistan will experience more than 15% (~6°C) increase in maximum land temperatures by the end of the 21st century relative to 2020. Significant increase in maximum LSTs and projected air temperature and humidity rise in Middle East (Pal & Eltahir, 2016) will stress resilience and adaptive capacities of the rapidly growing population in this region by end of the century. The socioeconomic
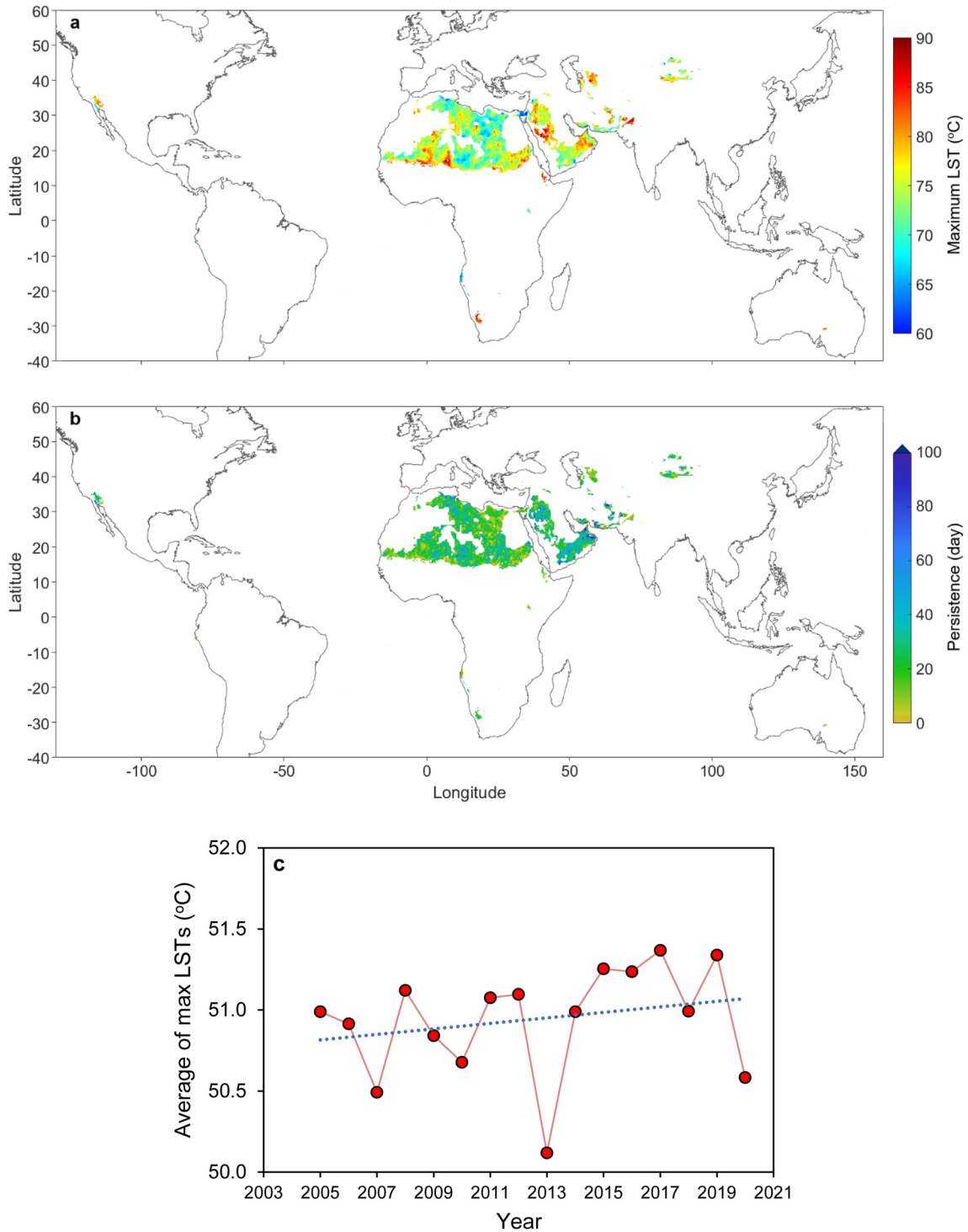
Figure 3. (a) Model estimates of the maximum temperature of hotspots during ~1,440 summer days (13:00 to 14:00 local time) from 2005 to 2020 depicting upper bounds of maximum LSTs; (b) number of days with temperatures greater than 90% of maximum land surface temperature of each map cell (pixel); (c) global average of maximum LSTs in hotspots from 2005 to 2020. Model outputs indicate that hotspots are warming at a rate of 0.17°C/decade.

effects associated with increasing LSTs will disproportionately harm low income regions (especially in North Africa) where life relies largely on crop production and livestock farming, similar to the impact of intensified heatwaves with global warming on suppressing economic growth of these often low emitting regions (Callahan & Mankin, 2022).
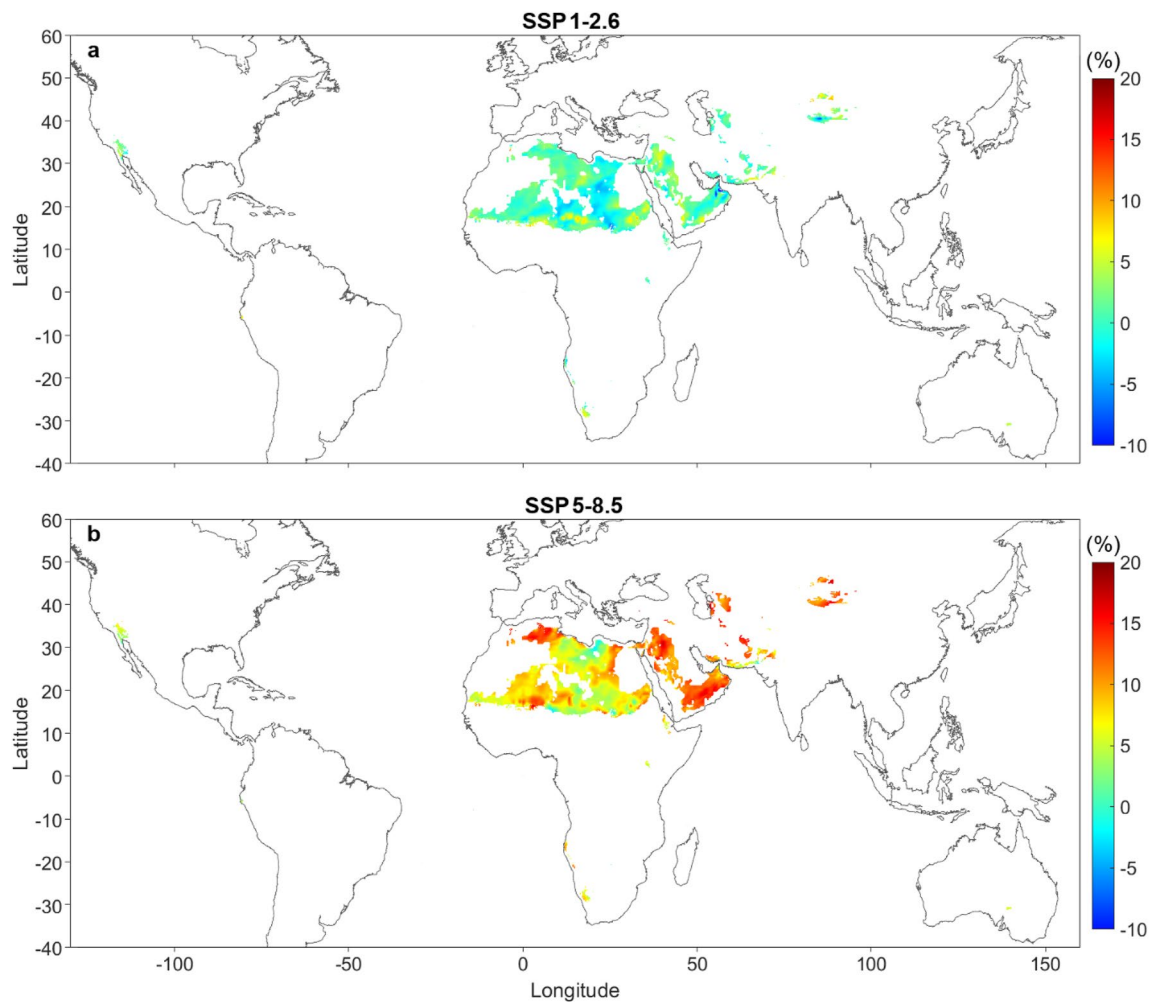
Figure 4. The percent changes in maximum land surface temperature of hotspots (in Degree Celsius) in 2100 relative to 2020 under SSP1-2.6 (a) and SSP5-8.5 (b) future climate scenarios indicating respective increase in radiative forcing of 2.6 and 8.5 W/m^2 in 2100.

4. Discussion

4.1. Ecological Implications of Maximum LST

The increase in LSTs with projected climate change (Figure 4) are expected to intensify lethal heatwaves, lead to human, plant, and animal thermal stresses, and cause crop and livestock failure. Although life sustaining and diverse hyper arid ecosystems are often overlooked (Azarderakhsh et al., 2020), recent study of Murali et al. (2023) highlights physiological limits of many species of vertebrates to extreme thermal stresses in the hot deserts of midlatitudes (and other habitats). Rapid changes in maximum LST in response to anthropogenic climate change can further limit life adaptation (primarily vegetation) to future hotter and harsher conditions in these ecosystems.

Regions with maximum LST are largely barren (reflecting water limitations and physiological constraints to vegetation (Nobel, 1984)). An important aspect of maximum LST effects on plant life is the magnitude, frequency, and persistence of extreme LST values over landscapes. Evidence suggests that most plant species (especially seedlings) are susceptible to irreversible heat damages such as protein denaturation, tissue browning, chlorophyll bleaching, and thus necrosis of plant tissues in temperatures exceeding 55°C (Haider et al., 2022; Hultine et al., 2023; Kolb & Robbrecht, 1996; Shaffique et al., 2022). Moreover, certain desert plant types can tolerate temperatures as high as 70°C (Nobel, 1984) supporting Nobel et al.'s (1986) predictions of plant survival exposed to soil surface temperatures of 74°C for 1 hr. This hard physiological limit to plant life adds importance to spatial delineation of limits of life under present and future climate. With this constraint in mind, we map the spatial distribution of hotspots that experienced maximum surface temperatures exceeding 75°C
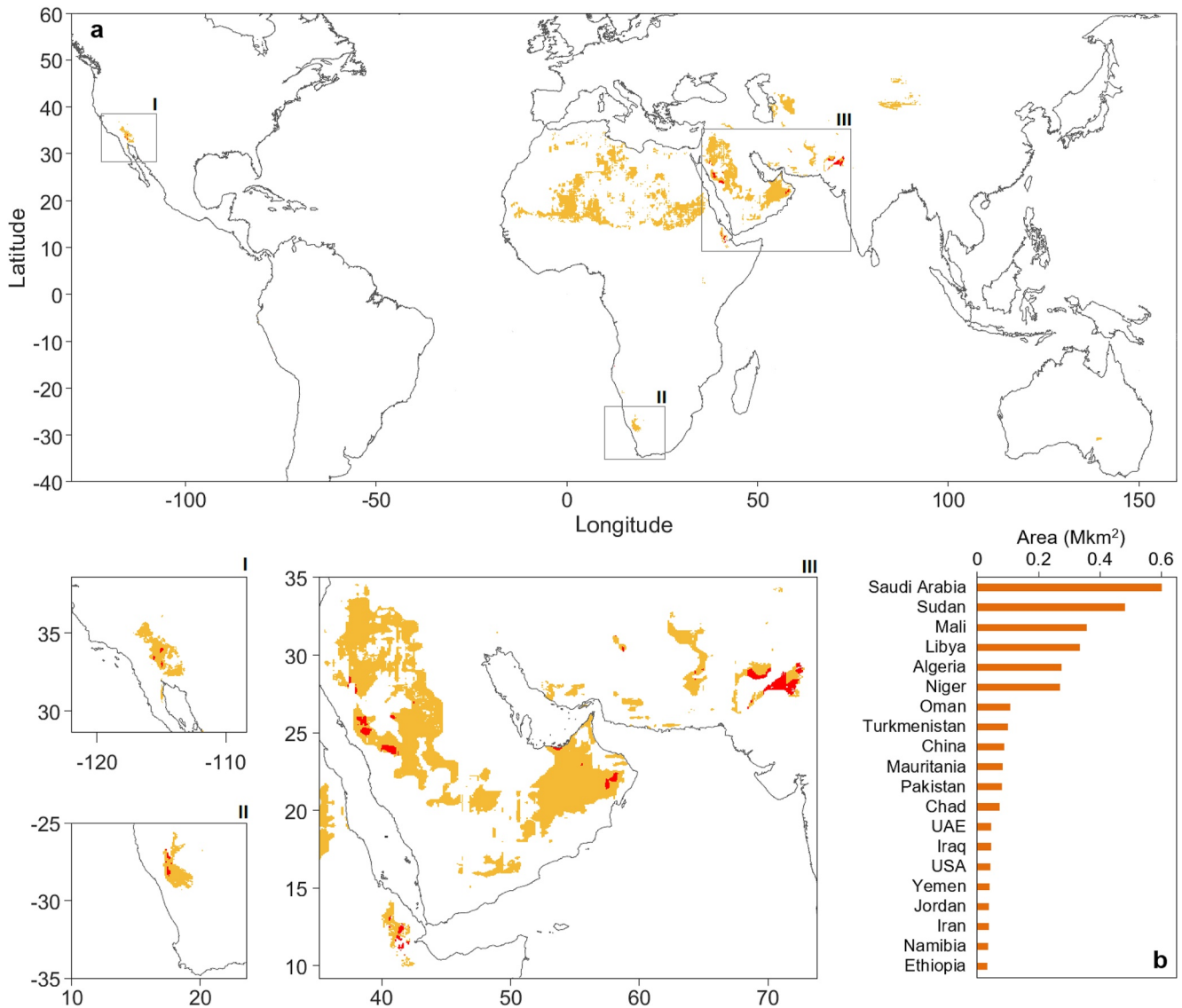
Figure 5. (a) Potentially inhospitable places for plant growth and succession (yellow areas) with surface temperatures exceeding 75°C over the study period from 2005 to 2020; red areas (highlighted in lower panels) mark hotspots where surface temperature (between 13:00 to 14:00 local time) exceeded 75°C for at least three consecutive days. (b) The top 20 countries with highest area of temperature hotspots (>75°C) that may limit plant life due to heat damages.

during the study period from 2005 to 2020 (we selected the higher value to provide a conservative estimate for locations that may limit plants survival due to heat damage). While hotspots with surface temperatures exceeding 75 °C are marked in yellow areas of Figure 5, persistence of such high values of surface temperatures (between 13:00 to 14:00 local time) for at least three consecutive days were observed in red areas. Temperature hotspots (>75°C) that may limit plant life are mainly located in Saudi Arabia (0.6 Mkm²), Sudan (0.48 Mkm²), Mali (0.36 Mkm²), Libya (0.34 Mkm²), Algeria (0.28 Mkm²), and Niger (0.27 Mkm²). The results in Figure 5 suggest potentially inhospitable places for plant growth and succession where high LSTs may suppress seed germination and seedlings require protected microhabitats (e.g., sheltered by adult plants) to survive heat stresses.

Increasing surface temperature with associated changes in diurnal temperature variations further influence the health and functioning of biocrusts serving as ecological and biogeochemical hotspots in arid regions (Antoninka et al., 2022; Belnap, 2013; Finger-Higgens et al., 2022). Our results delineate land temperature hotspots on the Earth under present and future climate conditions and shed new lights on ecological sustenance and biological adaptability in these often-unexplored places with limited accessibility.

4.2. Model Limitations, Uncertainties, and Perspectives for Future Research

The proposed physically based analytical framework will enable us to predict the global scale intensity and distribution of temperature extremes under different climate scenarios and quantify the future trends and patterns. This will contribute to devising the necessary action plans and implementing appropriate adaptation schemes. However, there are a few challenges and limitations associated with the proposed analytical framework listed below that could be addressed in future investigations.

- While global climate projections often provide climate data with spatial resolutions of 1-3° on a daily to monthly temporal basis, certain impact studies such as the extent of maximum LST here require highly resolved climate data at much higher temporal frequency. The occurrence of maximum LST is bounded to relatively short spells (i.e., 1–2 hr) (Sharifnezhadazizi et al., 2019). Additionally, inherent land heterogeneity and dynamic nature of meteorological forcing variables highlight the importance of climate data with high spatial resolutions (0.1–1 km) (Slingo et al., 2022) for predicting flash extreme events such as maximum LSTs. Considering the nonlinearity of underlying heat transfer processes, temporal integration of atmospheric variables could affect model predictions for future scenarios (Lim & Roderick, 2014) in Figure 4. To address this limitation, climate data with higher resolutions (in both time and space) are required (Shokri et al., 2023). The landmark climate informatic system planned to be generated within Destination Earth project (Bauer et al., 2021; Destination Earth, 2022) which aims to construct 1 km-scale "digital twins" of the Earth could be an ideal data set to be used in our framework.
- The predicted future temperature extremes highly depend on the reliability of the climate data. Future variations of climatic parameters depend on the climate models used to produce the data. As illustrated in Hassani et al. (2021), such differences in the outputs of climate models may result in even opposite predicted trends depending on the choice of the climate model. Therefore, the inherent degrees of uncertainty in the projected climate parameters influence our predictions of future temperature extremes.
- Global investigation of temperature hotspots (with 0.05°×0.05° spatial resolution) tacitly ignores the local radiative and aerodynamic adjustments arising from complex variation of land characteristics (e.g., surface undulations or yardang formations affecting turbulent interactions and shades (Heck et al., 2020)) and aspects of atmospheric stability to retain a simple, yet physically based analytic model for quantification of temperature extremes. Availability of highly resolved land characteristics allows incorporating these aspects in quantifying local temperature hotspots with higher spatial resolutions.

5. Conclusions

We proposed a simple analytical framework which capitalizes on land characteristics (land cover and elevation) and primary atmospheric forcing variables (wind and radiation) to globally identify hotspots for high land surface temperatures and their upper bounds. Our analysis identified more than 7.5 million km^2 barren surfaces susceptible for extremely high LSTs. The model indicated that hotspots mostly occur in midlatitudes between 13° to 43° (Middle East and North Africa) with surface temperatures that may exceed 85°C. Yearly analyses of maximum LSTs in summer days from 2005 to 2020 highlighted an increasing trend in maximum LSTs at a rate of 0.17°C/decade. The physically based approach enabled quantifying the extent of temperature hotspots in future for which we do not have satellite observations. Our future predictions under SSP5-8.5 indicated more than 15% (~6°C) increase in maximum temperature of hotspots by the end of the 21st century relative to 2020.

The study provides a theoretical basis for delineating the spatial extent of land hotspots and their impacts on regional climate extremes in a warmer future, and sheds lights on ecological sustenance and biological adaptability in these often-unexplored places with limited accessibility.

Conflict of Interest

The authors declare no conflicts of interest relevant to this study.

Data Availability Statement

The required data of the study explained in Section 2.2 were obtained from the following sources: MERRA-2 reanalyses meteorological data and surface thermal and radiative properties are available at Global Modeling and Assimilation Office (GMAO) (2015a, 2015b). Land cover data sets were obtained from Friedl and

Sulla-Menashe (2015). Soil type and bulk density data of HWSD were extracted from Wieder et al. (2014). Land elevation data are available at Danielson and Gesch (2011). Future climate data were obtained from NASA Earth Exchange Global Daily Downscaled Projections (NEX-GDDP-CMIP6) (2022).

References

Aminzadeh, M., & Or, D. (2013). Temperature dynamics during nonisothermal evaporation from drying porous surfaces. *Water Resources Research*, *49*(11), 7339–7349. https://doi.org/10.1002/2013WR014384

Aminzadeh, M., & Or, D. (2014). Energy partitioning dynamics of drying terrestrial surfaces. *Journal of Hydrology*, *519*, 1257–1270. https://doi.org/10.1016/j.jhydrol.2014.08.037

Aminzadeh, M., & Or, D. (2017). The complementary relationship between actual and potential evaporation for spatially heterogeneous surfaces. *Water Resources Research*, *53*(1), 580–601. https://doi.org/10.1002/2016WR019759

Aminzadeh, M., Roderick, M. L., & Or, D. (2016). A generalized complementary relationship between actual and potential evaporation defined by a reference surface temperature. *Water Resources Research*, *52*(1), 385–406. https://doi.org/10.1002/2015WR017969

Aminzadeh, M., Roderick, M. L., & Or, D. (2021). Using the complementary relationship between actual and potential evaporation to diagnose the onset of heatwaves. *Water Resources Research*, *57*(11), e2020WR029156. https://doi.org/10.1029/2020WR029156

Antoninka, A., Chuckran, P. F., Mau, R. L., Slate, M. L., Mishler, B. D., Oliver, M. J., et al. (2022). Responses of biocrust and associated soil bacteria to novel climates are not tightly coupled. *Frontiers in Microbiology*, *13*. https://doi.org/10.3389/fmicb.2022.821860

Azarderakhsh, M., Prakash, S., Zhao, Y., & AghaKouchak, A. (2020). Satellite-based analysis of extreme land surface temperatures and diurnal variability across the hottest place on Earth. *IEEE Geoscience and Remote Sensing Letters*, *17*(12), 2025–2029. https://doi.org/10.1109/LGRS.2019.2962055

Bauer, P., Stevens, B., & Hazeleger, W. (2021). A digital twin of Earth for the green transition. *Nature Climate Change*, *11*(2), 80–83. https://doi.org/10.1038/s41558-021-00986-y

Belnap, J. (2013). Some like it hot, some not. *Science*, *340*(6140), 1533–1534. https://doi.org/10.1126/science.1240318

Brutsaert, W. (1982). *Evaporation into the atmosphere*. Springer Netherlands. https://doi.org/10.1007/978-94-017-1497-6

Büntgen, U., Urban, O., Krusic, P. J., Rybníček, M., Kolář, T., Kyncl, T., et al. (2021). Recent European drought extremes beyond Common Era background variability. *Nature Geoscience*, *14*(4), 190–196. https://doi.org/10.1038/s41561-021-00698-0

Callahan, C. W., & Mankin, J. S. (2022). Globally unequal effect of extreme heat on economic growth. *Science Advances*, *8*(43), eadd3726. https://doi.org/10.1126/sciadv.add3726

Chen, Y., Yang, K., He, J., Qin, J., Shi, J., Du, J., & He, Q. (2011). Improving land surface temperature modeling for dry land of China. *Journal of Geophysical Research*, *116*(D20), D20104. https://doi.org/10.1029/2011JD015921

Danielson, J. J., & Gesch, D. B. (2011). Global multi-resolution Terrain elevation data 2010 (GMTED2010): U.S Geological Survey Open-File Report 2011-1073 (26 p.) [Dataset]. https://doi.org/10.3133/ofr20111073

Destination Earth Shaping Europe's digital future. (2022). Retrieved from https://digital-strategy.ec.europa.eu/en/policies/destination-earth

Finger-Higgens, R., Duniway, M. C., Fick, S., Geiger, E. L., Hoover, D. L., Pfennigwerth, A. A., et al. (2022). Decline in biological soil crust N-fixing lichens linked to increasing summertime temperatures. *Proceedings of the National Academy of Sciences*, *119*(16), e2120975119. https://doi.org/10.1073/pnas.2120975119

Friedl, M., & Sulla-Menashe, D. (2015). MCD12C1 MODIS/Terra+Aqua land cover type yearly L3 global 0.05Deg CMG V006 [Dataset]. NASA EOSDIS Land Processes DAAC. https://doi.org/10.5067/MODIS/MCD12C1.006

Garratt, J. R. (1992). Extreme maximum land surface temperatures. *Journal of Applied Meteorology*, *31*(9), 1096–1105. https://doi.org/10.1175/1520-0450(1992)031<1096:emlst>2.0.co;2

Gelaro, R., McCarty, W., Suárez, M. J., Todling, R., Molod, A., Takacs, L., et al. (2017). The Modern-Era retrospective analysis for Research and Applications, version 2 (MERRA-2). *Journal of Climate*, *30*(14), 5419–5454. https://doi.org/10.1175/JCLI-D-16-0758.1

Global Modeling and Assimilation Office (GMAO). (2015a). MERRA-2 inst1_2d_lfo_Nx: 2d, 1-Hourly, Instantaneous, Single-Level, Assimilation, Land Surface Forcings V5.12.4, Greenbelt, MD, USA, Goddard Earth Sciences Data and Information Services Center (GES DISC) [Dataset]. Retrieved from https://disc.gsfc.nasa.gov/datasets/M2I1NXLFO_5.12.4/summary

Global Modeling and Assimilation Office (GMAO). (2015b). MERRA-2 tavg1_2d_rad_Nx: 2d, 1-Hourly,Time-Averaged, Single-Level,Assimilation, Radiation Diagnostics V5.12.4, Greenbelt, MD, USA, Goddard Earth Sciences Data and Information Services Center (GES DISC) [Dataset]. Retrieved from https://disc.gsfc.nasa.gov/datasets/M2T1NXRAD_5.12.4/summary

Haghighi, E., & Or, D. (2013). Evaporation from porous surfaces into turbulent airflows: Coupling eddy characteristics with pore scale vapor diffusion. *Water Resources Research*, *49*(12), 8432–8442. https://doi.org/10.1002/2012WR013324

Haider, S., Iqbal, J., Naseer, S., Shaukat, M., Abbasi, B. A., Yaseen, T., et al. (2022). Unfolding molecular switches in plant heat stress resistance: A comprehensive review. *Plant Cell Reports*, *41*(3), 775–798. https://doi.org/10.1007/s00299-021-02754-w

Hassani, A., Azapagic, A., & Shokri, N. (2021). Global predictions of primary soil salinization under changing climate in the 21st century. *Nature Communications*, *12*(1), 6663. https://doi.org/10.1038/s41467-021-26907-3

He, H., Liu, L., Dyck, M., Si, B., & Lv, J. (2021). Modelling dry soil thermal conductivity. *Soil and Tillage Research*, *213*, 105093. https://doi.org/10.1016/j.still.2021.105093

Heck, K., Coltman, E., Schneider, J., & Helmig, R. (2020). Influence of radiation on evaporation rates: A numerical analysis. *Water Resources Research*, *56*(10), e2020WR027332. https://doi.org/10.1029/2020WR027332

Herrero, J., & Polo, M. J. (2012). Parameterization of atmospheric longwave emissivity in a mountainous site for all sky conditions. *Hydrology and Earth System Sciences*, *16*(9), 3139–3147. https://doi.org/10.5194/hess-16-3139-2012

Hobbins, M. T., Ramírez, J. A., Brown, T. C., & Claessens, L. H. J. M. (2001). The complementary relationship in estimation of regional evapotranspiration: The complementary relationship areal evapotranspiration and advection-aridity models. *Water Resources Research*, *37*(5), 1367–1387. https://doi.org/10.1029/2000WR900358

Hultine, K. R., Hernández-Hernández, T., Williams, D. G., Albeke, S. E., Tran, N., Puente, R., & Larios, E. (2023). Global change impacts on cacti (Cactaceae): Current threats, challenges and conservation solutions. *Annals of Botany*. https://doi.org/10.1093/aob/mcad040

Jury, W. A., & Horton, R. (2004). *Soil physics*. John Wiley & Sons.

Kolb, P. F., & Robberecht, R. (1996). High temperature and drought stress effects on survival of Pinus ponderosa seedlings. *Tree Physiology*, *16*(8), 665–672. https://doi.org/10.1093/treephys/16.8.665

Kubecka, P. (2001). A possible world record maximum natural ground surface temperature. *Weather*, *56*(7), 218–221. https://doi.org/10.1002/j.1477-8696.2001.tb06577.x

Lacis, A. A., Schmidt, G. A., Rind, D., & Ruedy, R. A. (2010). Atmospheric CO2: Principal control knob governing Earth's temperature. *Science*, *330*(6002), 356–359. https://doi.org/10.1126/science.1190653

Lehmann, P., Assouline, S., & Or, D. (2008). Characteristic lengths affecting evaporative drying of porous media. *Physical Review E: Statistical, Nonlinear, and Soft Matter Physics*, *77*(5 Pt 2), 056309. https://doi.org/10.1103/PhysRevE.77.056309

Lehmann, P., Berli, M., Koonce, J. E., & Or, D. (2019). Surface evaporation in arid regions: Insights from lysimeter decadal record and global application of a surface evaporation capacitor (SEC) model. *Geophysical Research Letters*, *46*(16), 9648–9657. https://doi.org/10.1029/2019GL083932

Li, Z.-L., Tang, B.-H., Wu, H., Ren, H., Yan, G., Wan, Z., et al. (2013). Satellite-derived land surface temperature: Current status and perspectives. *Remote Sensing of Environment*, *131*, 14–37. https://doi.org/10.1016/j.rse.2012.12.008

Lim, W. H., & Roderick, M. L. (2014). Up-scaling short-term process-level understanding to longer timescales using a covariance-based approach. *Hydrology and Earth System Sciences*, *18*(1), 31–45. https://doi.org/10.5194/hess-18-31-2014

Masson-Delmotte, V., Zhai, P., Pirani, A., Connors, S. L., Péan, C., Chen, Y., et al. (2021). IPCC (2021), climate change 2021: The physical science basis. Contribution to the sixth Assessment Report of the intergovernmental panel on climate change (p. 16).

Mauritsen, T., Bader, J., Becker, T., Behrens, J., Bittner, M., Brokopf, R., et al. (2019). Developments in the MPI-M Earth system model version 1.2 (MPI-ESM1.2) and its response to increasing CO2. *Journal of Advances in Modeling Earth Systems*, *11*(4), 998–1038. https://doi.org/10.1029/2018MS001400

Mildrexler, D. J., Zhao, M., & Running, S. W. (2011). Satellite finds highest land skin temperatures on Earth. *Bulletin of the American Meteorological Society*, *92*(7), 855–860. https://doi.org/10.1175/2011BAMS3067.1

Miralles, D. G., Teuling, A. J., van Heerwaarden, C. C., & de Vilà-Guerau Arellano, J. (2014). Mega-heatwave temperatures due to combined soil desiccation and atmospheric heat accumulation. *Nature Geoscience*, *7*(5), 345–349. https://doi.org/10.1038/ngeo2141

Murali, G., Iwamura, T., Meiri, S., & Roll, U. (2023). Future temperature extremes threaten land vertebrates. *Nature*, *615*(7952), 1–7. https://doi.org/10.1038/s41586-022-05606-z

NASA Earth Exchange Global Daily Downscaled Projections (NEX-GDDP-CMIP6). (2022). [Dataset]. Retrieved from https://www.nccs.nasa.gov/services/data-collections/land-based-products/nex-gddp-cmip6

NCEI. (2022). National Centers for Environmental information (NCEI). Retrieved from https://www.ncei.noaa.gov/access/monitoring/global-temperature-anomalies/anomalies

Nobel, P. S. (1984). Extreme temperatures and thermal tolerances for seedlings of desert succulents. *Oecologia*, *62*(3), 310–317. https://doi.org/10.1007/BF00384262

Nobel, P. S., Geller, G. N., Kee, S. C., & Zimmerman, A. D. (1986). Temperatures and thermal tolerances for cacti exposed to high temperatures near the soil surface. *Plant, Cell and Environment*, *9*(4), 279–287. https://doi.org/10.1111/1365-3040.ep11611688

Pal, J. S., & Eltahir, E. A. B. (2016). Future temperature in southwest Asia projected to exceed a threshold for human adaptability. *Nature Climate Change*, *6*(2), 197–200. https://doi.org/10.1038/nclimate2833

Pietikäinen, J., Pettersson, M., & Bååth, E. (2005). Comparison of temperature effects on soil respiration and bacterial and fungal growth rates. *FEMS Microbiology Ecology*, *52*(1), 49–58. https://doi.org/10.1016/j.femsec.2004.10.002

Riahi, K., van Vuuren, D. P., Kriegler, E., Edmonds, J., O'Neill, B. C., Fujimori, S., et al. (2017). The Shared Socioeconomic Pathways and their energy, land use, and greenhouse gas emissions implications: An overview. *Global Environmental Change*, *42*, 153–168. https://doi.org/10.1016/j.gloenvcha.2016.05.009

Shaffique, S., Khan, M. A., Wani, S. H., Pande, A., Imran, M., Kang, S.-M., et al. (2022). A review on the role of Endophytes and plant growth promoting rhizobacteria in mitigating heat stress in plants. *Microorganisms*, *10*(7), 1286. https://doi.org/10.3390/microorganisms10071286

Shahraeeni, E., & Or, D. (2011). Quantification of subsurface thermal regimes beneath evaporating porous surfaces. *International Journal of Heat and Mass Transfer*, *54*(19), 4193–4202. https://doi.org/10.1016/j.ijheatmasstransfer.2011.05.024

Sharifnezhadazizi, Z., Norouzi, H., Prakash, S., Beale, C., & Khanbilvardi, R. (2019). A global analysis of land surface temperature diurnal cycle using MODIS observations. *Journal of Applied Meteorology and Climatology*, *58*(6), 1279–1291. https://doi.org/10.1175/JAMC-D-18-0256.1

Shokri, N., & Or, D. (2011). What determines drying rates at the onset of diffusion controlled stage-2 evaporation from porous media? *Water Resources Research*, *47*(9). https://doi.org/10.1029/2010WR010284

Shokri, N., Stevens, B., Madani, K., Grabe, J., Schlüter, M., & Smirnova, I. (2023). Climate informed Engineering: An Essential pillar of industry 4.0 transformation. *ACS Engineering Au*, *3*(1), 3–6. https://doi.org/10.1021/acsengineeringau.2c00037

Slingo, J., Bates, P., Bauer, P., Belcher, S., Palmer, T., Stephens, G., et al. (2022). Ambitious partnership needed for reliable climate prediction. *Nature Climate Change*, *12*(6), 499–503. https://doi.org/10.1038/s41558-022-01384-8

Stone, R. (2016). Some like it hot. *Science*, *354*(6318), 1366–1368. https://doi.org/10.1126/science.354.6318.1366

Thrasher, B., Wang, W., Michaelis, A., Melton, F., Lee, T., & Nemani, R. (2022). NASA global daily downscaled projections, CMIP6. *Scientific Data*, *9*(1), 262. https://doi.org/10.1038/s41597-022-01393-4

Tran, D. X., Pla, F., Latorre-Carmona, P., Myint, S. W., Caetano, M., & Kieu, H. V. (2017). Characterizing the relationship between land use land cover change and land surface temperature. *ISPRS Journal of Photogrammetry and Remote Sensing*, *124*, 119–132. https://doi.org/10.1016/j.isprsjprs.2017.01.001

Wang, H., Zhang, J., Chen, L., & Li, D. (2022). Relationship between summer extreme precipitation anomaly in Central Asia and surface sensible heat variation on the Central-Eastern Tibetan Plateau. *Climate Dynamics*, *59*(3), 685–700. https://doi.org/10.1007/s00382-022-06148-w

Webb, M. J., Andrews, T., Bodas-Salcedo, A., Bony, S., Bretherton, C. S., Chadwick, R., et al. (2017). The Cloud Feedback Model Intercomparison Project (CFMIP) contribution to CMIP6. *Geoscientific Model Development*, *10*(1), 359–384. https://doi.org/10.5194/gmd-10-359-2017

Wieder, W. R., Boehnert, J., Bonan, G. B., & Langseth, M. (2014). Regridded harmonized world soil Database v1.2 [Dataset]. https://doi.org/10.3334/ORNLDAAC/1247

Zhao, Y., Norouzi, H., Azarderakhsh, M., & AghaKouchak, A. (2021). Global patterns of hottest, coldest, and extreme diurnal variability on Earth. *Bulletin of the American Meteorological Society*, *102*(9), E1672–E1681. https://doi.org/10.1175/BAMS-D-20-0325.1